ELSEVIER

Polymer 42 (2001) 9059–9071

polymer

www.elsevier.com/locate/polymer

Structure–property-processing investigations of the tenter-frame process for making biaxially oriented HDPE film. I. Base sheet and draw along the MD

Varun Ratta[a,1], Garth L. Wilkes[a,*], T.K. Su[b]

[a]*Polymer Materials and Interfaces Laboratory, Department of Chemical Engineering, Virginia Polytechnic Institute, State University, Blacksburg, VA 24061, USA*
[b]*Exxon Mobil Chemical Company, Macedon, NY 14502, USA*

Received 2 March 2001; received in revised form 1 May 2001; accepted 1 May 2001

Abstract

We discuss here the first two stages of the tenter-frame film manufacturing process for HDPE, viz. (a) the extrusion of the polymer onto a cooled cast roll (base sheet) and (b) drawing along the machine direction (MD) using several sets of rolls (referred to as machine draw orientation (MDO) sheet). The structure–property relationships are analyzed for a single resin when the cast-roll temperature, MDO temperature and MD draw ratio are systematically varied. The thick base sheets were made by extrusion onto a cast roll at three different temperatures of T_b, $T_b - 11°C$ and $T_b + 11°C$ (T_b being a reference temperature for the base-sheet draw). While the WAXD indicated an unoriented system, atomic force microscopy (AFM) and transmission electron microscopy (TEM) revealed spherulites of ca. 3–5 μm diameter across the thickness of this base sheet. DSC indicated that the base sheet possessed a broad distribution of lamellar thickness and had a degree of crystallinity (X_c) of ca. 75%. After drawing 6*X* along the MD at three different drawing temperatures, of T_{MDO}, $T_{MDO} - 8°C$ and $T_{MDO} + 8°C$ (T_{MDO} being a reference temperature for the MDO-sheet draw), both AFM and TEM revealed a complete change in morphology to well-developed lamellar stacks oriented perpendicular to the MD. The MD draw ratio was then systematically varied from 1.5*X*, 2.25*X*, 3*X*, 4.5*X* to 6*X*, while keeping the other processing variables constant to understand how transformation of the spherulites to a stacked lamellar morphology took place. A very systematic change in morphology and orientation of the MDO sheet was observed with changing draw ratios, while the degree of crystallinity did not change. For the conditions utilized, the draw ratio of 2.25*X* was enough to destroy the general features of the bulk spherulitic superstructure although the broken and deformed lamellar remnants of the spherulites remained. With higher draw ratios, well-stacked lamellar structures oriented perpendicular to MD were gradually introduced at the expense of the deformed lamellae. At a draw ratio of 6*X*, only stacked lamellar structures were present. We discuss the causes of this transformation from primarily three standpoints: (a) localized melting and recrystallization followed by microfibrillation, (b) bulk melting followed by row nucleation and (c) a combination of the above two mechanisms. Interestingly, both X-ray and refractive index measurements revealed that the MDO process resulted in some level of biaxial orientation of the crystal phase. This arises due to the nature of the MDO process, which places constraints on the narrowing of the transverse dimensions during drawing.

Keywords: Linear polyethylene; Orientation; Tenter process

1. Introduction

Polymers like polypropylene and polyethylene are widely used as flexible films for food packaging applications. In fact, this represents a more than $5 billion industry today [1]. These food-packaging applications, however, place stringent demands on the properties of the final polymer film. While properties such as haze and gloss are important from an aesthetic standpoint, barrier properties like oxygen transmission rate (OTR) and water vapor transmission rate (WVTR) are important for increasing the 'shelf-life' of the packaged materials [2]. In addition, the right combination of mechanical properties (e.g. modulus and elongation to yield/break) and thermal properties (e.g. heat sealing and shrinkage) is also required. To achieve the desired properties and make better packaging films, it is important to understand how the processing variables affect the film crystallization, orientation and morphology and how this

* Corresponding author. Tel.: +1-540-231-5498; fax: +1-540-231-9511.
E-mail address: gwilkes@vt.edu (G.L. Wilkes).
[1] Present address: Dow Chemical Company, Freeport, TX, USA.

0032-3861/01/$ - see front matter
PII: S0032-3861(01)00387-1

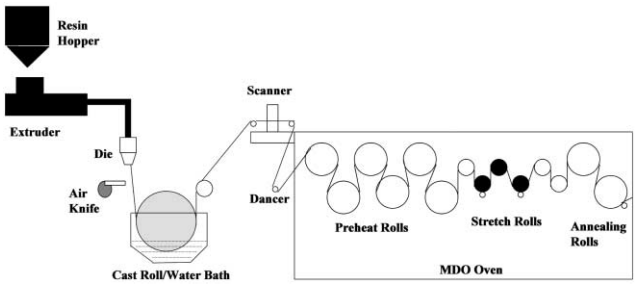

Fig. 1. Extrusion of the polymer to a cast roll and MDO drawing process using set of heated rolls.

orientation/morphology correlates with the final film properties. From a commercial standpoint, the two primary routes by which these films are manufactured are (a) the 'tenter-frame process' — a sequential or simultaneous process in which the polymer melt is first melt extruded onto a cast roll, and then stretched sequentially or simultaneously in the 'machine direction' (MD) and the 'transverse direction' (TD) and (b) the 'blown-film process', where the final film results by biaxially blowing the molten polymer tube into a larger diameter bubble. Among the tenter-frame processes, the sequential step-by-step biaxial drawing method is more commonly practiced throughout the world [3]. While several characterization studies in the literature discuss the details of the blown-film process [4–15] and the tenter-frame process for PET [16], the 'tenter-frame process for HDPE' remains scantily discussed [17] from a morphological and orientation standpoint. The main advantages of the tenter-frame process over the blown-film' process include significantly faster production times, flexibility in change of process conditions and better control over the final film thickness [2,18]. While there are a large number of excellent studies in the literature discussing the deformation of an unoriented semicrystalline polymer and the related orientation effects [19–31], this work to our knowledge, is among the first focusing on the sequential tenter-frame process for HDPE.

In a continuous manufacturing method such as the tenter-frame process, the structure and properties of the film at each stage of manufacturing may have a direct or indirect influence on the final film structure. Thus, for example, the structure of the 'base sheet' obtained after the cast roll may influence the structure of the 'machine draw orientation (MDO) sheet' and the structure of MDO sheet may, in turn, have a substantial affect on the structure of the TD oriented final film. It is generally realized in this regard that the 'drawability' and 'uniformity of drawing' of the base sheet to an MDO sheet is increased if the crystallinity can be decreased and if large spherulites are prevented from forming. Thus, rapid quenching is often necessary in industrial operations and can be achieved by keeping the cast-roll temperature low. For the MD draw process, while the end requirements from a structural standpoint are less understood, it is usually required that the draw temperature, line speed and draw ratios are such so that a precursor sheet of uniform thickness and uniform optical properties is produced for the TD drawing step. To tailor final films for a specific application, it is important to understand these relationships concerning the processing conditions and how they affect the morphology at each stage of manufacture. In this study, we address some of the questions concerning the effect of certain processing variables on the structure of the drawn HDPE film. We specifically focus our attention on the first two stages of the tenter-frame process concerning the production of the base sheet and the MDO sheet.

Fig. 1 shows the manufacturing scheme and identifies some of the key processing variables that affect the structure and properties of the film during the first two stages of this process. The full list of variables include (1) molecular weight, molecular weight distribution, and configurational aspects of the resin used, (2) cast-roll temperature, (3) line speed, (4) drawing temperature in the MD (henceforth referred as MDO temperature in this paper), (5) MD draw ratio. Other processing parameters that are important but not discussed within this report are the drawing temperature in the TD, TD draw ratio and the final-film thickness. In addition, several other subtle variables such as how the draw is carried out in each stage (i.e. in one step or in several steps) or other factors like manufacturing a multilayered film can affect the structure/properties of the final film. To understand the influence of so many variables, the manufacturing parameters need to be systematically varied. The tenter-frame process provides more flexibility in altering the process variables than the traditional blown film process [3]. However, even in the tenter-frame process, these parameters cannot be freely changed if the manufacturing process is to be feasible on an industrial scale. Thus, the variation of these processing parameters can only take place in the window that allows the production of an economically viable final film. While keeping the resin unchanged, this paper specifically focuses on the first two stages of this film manufacturing process and discusses the effect of critical variables such as cast-roll temperature, MDO draw temperature and MDO draw ratio on the orientation and morphology of the intermediate films. It is pointed out that due to proprietary aspects, the specific temperature utilized will not be given but the spread in temperature will be provided. A subsequent publication will discuss the detailed results dealing with the transverse-draw stage of this manufacturing process.

2. Experimental

The linear HDPE used in this study had a $\langle M_n \rangle$ of 20,000 g/mol, $\langle M_w \rangle$ of 153,000 g/mol and $\langle M_z \rangle$ of 1,152,000 g/mol as determined by GPC. DSC experiments were conducted on a Perkin–Elmer DSC7 using 2 mg of sample in a nitrogen atmosphere. A heating rate of

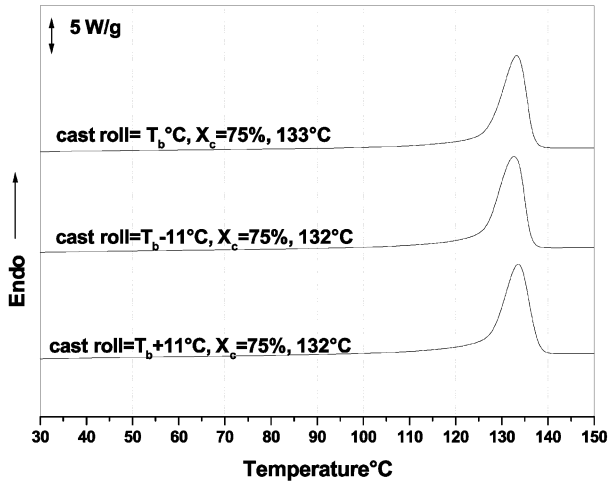

Fig. 2. The melting profile, peak melting points and degree of crystallinity of the various base sheets. No appreciable differences were observed for variation in cast-roll temperature.

30°C/min was utilized and calibration was carried out using indium and tin standards. Atomic force microscopy (AFM) was conducted in tapping mode using Nanoscope III®, Dimension 3000 scanning probe microscope from Digital Instruments. Both the base sheet and the MDO sheet were manufactured with a very thin layer of ethylene–propylene (EP) copolymer 'skin' on both sides of the sheet/film. This skin was slowly peeled off prior to any microscopy experiment. AFM experiments were performed on the surface of the base/MDO sheet after this layer was removed. As will be shown later, this EP skin did not have any influence on the morphological features of the underlying polyethylene material. Wide-angle X-ray scattering (WAXS) were performed using a Philips tabletop X-ray generator (Model PW 1720) with CuK_α radiation ($\lambda = 1.54$ Å) and equipped with a standard vacuum-sealed Warhus photographic pinhole camera. The instrument was operated at 40 kV and 20 mA. In order to obtain X-ray scattering through the thickness (for MDO-sheet samples), thin sections were carefully cut and stacked together. In order to determine the refractive index in all three dimensions, i.e. MD (z), TD (y) and ND (x), a METRICON prism coupler refractometer Model 2010, equipped with a polarized laser beam was utilized.[2] The samples were accurately marked for directions and three to five readings were taken for each sample for slight variations in the placement direction of the film. For transmission electron microscopy (TEM), samples were stained using chlorosulfonic acid at 60°C for 6–10 h, washed with concentrated sulfuric acid and water, and then dried overnight [32–35]. Subsequently, the samples were embedded in epoxy and ultramicrotomed using a diamond knife to obtain sections of ca. 70–100 nm thicknesses. For many of the samples, thin sections were first carefully sliced under a microscope before staining was conducted. Subsequent to ultramicrotomy, all samples were stained in a 0.7% solution of uranyl acetate overnight. The TEM was performed across the complete thickness profile so as detect any possible differences between the morphology at the surfaces and within the bulk of the specimen.

[2] For more information, see http://www.metricon.com.

3. Results and discussion

3.1. Base-sheet results

The base sheet serves as a precursor to the machine draw and transverse draw stages. It results from the extrusion of the molten polymer onto the water-cooled cast roll so as to give a 1500 μm thick sheet. After the extrusion, an air-knife presses the molten polymer against the cast roll. The frost line develops on the extruded HDPE when it is pressed against the cast rolls, but before it contacts the water bath on the outer side. This relatively thick base sheet subsequently leads to an MDO sheet after a 6*X* MDO draw and final film after a TD draw. Usually, it is required that fast quenching occurs so as to yield a precursor sheet with the least degree of crystallinity and a small spherulitic size. These properties result in a film that can be more easily drawn along the MD. In this regard, the cast-roll temperature was one of the parameters that was controlled at either T_b, $T_b - 11$°C and $T_b + 11$°C. While the cast-roll temperature was the operating parameter controlled in this instance, the overall crystallization process of the resin was still non-isothermal. As the resin was extruded, it underwent cooling first by the air-knife, then by the cast roll (inner side of the sheet) and finally also by the water bath (that contacts the outer surface). The base sheets, so obtained, were analyzed for melting behavior, crystallinity, morphology and orientation. The melting curves for the various base sheets are shown in Fig. 2. The melting profile of all the samples is very similar to peak melting points of ca.132°C and the average crystallinity of ca. 75%. The partial melting and recrystallization during the DSC heating scan may erase some of the finer differences among these samples. An error of 0.1 mg associated with the weighing of our samples will also affect this calculation by ca. ±3%. For these reasons, the degree of crystallinity calculated from the melting curves is approximate.

Fig. 3 shows the WAXD scans for the base sheets when the X-ray was passed parallel to the normal direction. The very intense (110) and (200) reflections from the orthorhombic unit cell of the PE ($a = 7.40$ Å, $b = 4.93$ Å, $c = 2.54$ Å) are clearly visible in all the samples along with weaker reflections from other planes. As expected, no evidence of any orientation (azimuthal dependence) along the MD is observed for any of the samples. The intensity of the X-ray patterns is also similar supporting the early deduction that there were not any major differences (±3%) in the level of crystallinity among the various samples. The base sheet was then examined for differences in morphology using

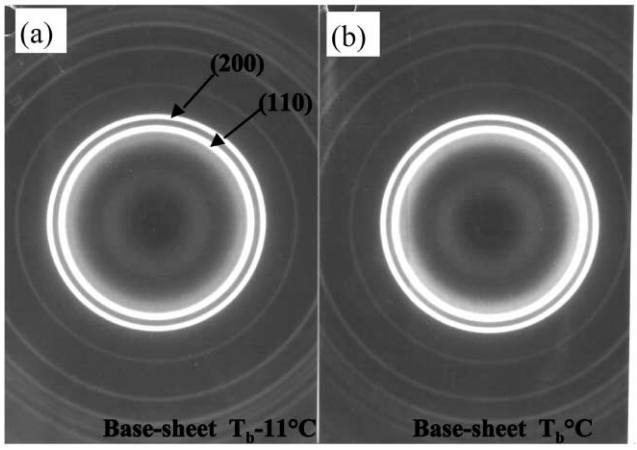

Fig. 3. WAXD scans for two typical base sheets for which the cast-roll temperatures were (a) $T_b - 11$°C and (b) T_b°C.

AFM and TEM. While the AFM yielded information about the surfaces in contact with the cast roll (top) and the water bath (bottom), the TEM in different regions of the samples gave information about the morphology near the surface as well in the bulk of the sample. Spherulitic morphology was observed for all the base sheet samples with average spherulitic size of ca. 3–5 μm on the surface using the AFM (Fig. 4). TEM within the bulk of the HDPE sheet (Fig. 5a) revealed very well-defined spherulitic superstructure of approximately the same size. The higher resolution TEM micrographs (Fig. 5b) demonstrate well-developed stacks of twisted lamellae within the spherulites. Also, in accord with the WAXD results, the morphology does not suggest any orientation to be present. The AFM reveals a coarse and irregularly developed spherulitic morphology, which is partially caused by the cast and other rolls that press against

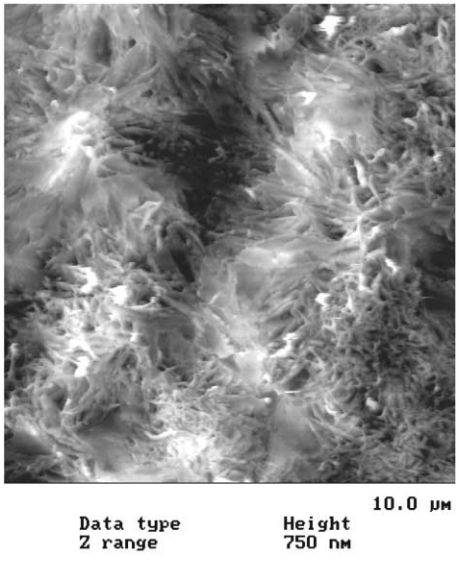

Fig. 4. AFM height image for a typical base sheet. The size of the image is 10 μm × 10 μm. *Z*-range of 750 nm indicates the difference in heights between the brightest and darkest regions.

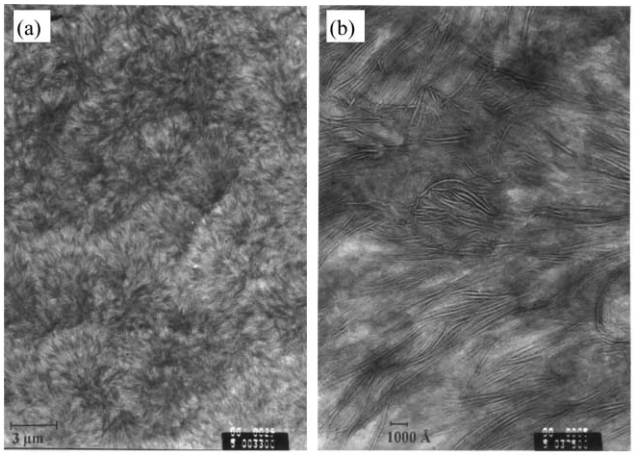

Fig. 5. (a) TEM showing the spherulitic morphology in a typical base sheet resin. The average size of the spherulites is ca. 3–5 μm. (b) Higher resolution TEM near a spherulitic boundary and showing stacks of lamellae within the spherulite.

both surfaces of the base sheet during the manufacturing process. The size of the spherulites within a given sample did not show any significant differences across the thickness of the sheet, thereby somewhat surprisingly indicating good heat transfer through the sheet. In this regard, it is useful to mention that the 'frost-line' during the manufacturing process is observed on the sheet in contact with the cast roll before it touches the water bath, thereby indicating the initiation of the nucleation and substantial development of crystallinity before the sheet comes in contact with the water. However, it was surprising to note that in the 22°C range of cast-roll temperatures utilized in the present study, no significant differences were observed in spherulitic size. These results also confirm that the EP skin did not have any noticeable effect on the surface morphology (spherulitic size). From a practical standpoint, these results lead to the conclusion that the cast-roll temperature may be a less critical variable to control in this process in the range of temperatures used here. The results also suggest that stronger quenching procedures might be utilized to obtain further reduction in the degree of crystallinity of the base sheet if desired.

3.2. MDO-sheet results

The next step in the film manufacturing process involves the MD draw of the base sheet after passing through a series of heated rolls. Initially for this step, the MD draw was fixed at 6*X* and the draw temperature was set at T_{MDO}, $T_{MDO} - 9$°C, $T_{MDO} + 9$°C. All the drawing temperatures are located in the region of bulk melting of the polyethylene. While the draw temperatures of T_{MDO} and $T_{MDO} - 9$°C, are located on the lower temperature side of the primary melting endotherm, the draw temperature of $T_{MDO} + 9$°C is positioned after the peak melting point. DSC was conducted at 30°C/min (to minimize reorganization) on small samples

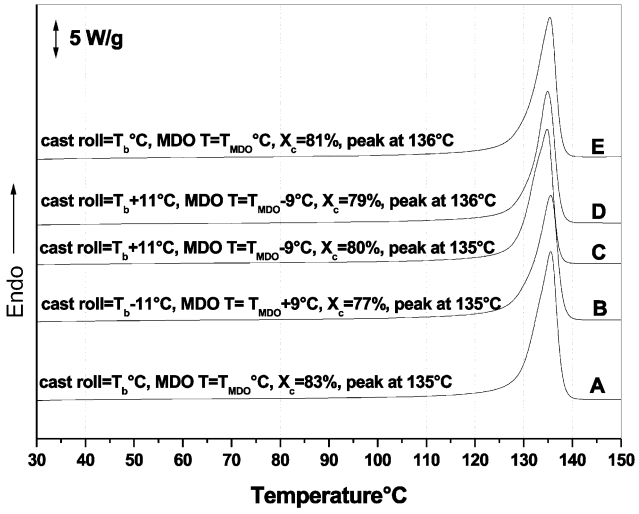

Fig. 6. DSC melting profile of various MDO sheets at 30°C/min. The relative cast-roll temperature, the relative MD draw temperature, the degree of crystallinity calculated from the DSC curves and the peak melting points are listed, respectively.

(2 mg) to minimize any heat transfer problems (Fig. 6). It is noticed that a significant sharpening of the overall melting profile takes place following the 6*X* draw with a noticeable increase in the peak melting temperature (135–136°C). This suggests a narrow distribution of more perfect and thicker lamellar crystals in the MDO sheet than in the precursor base sheet. However, it is a bit surprising that there are no appreciable differences in the melting profile of the various MDO-sheet samples. Further WAXS results and their discussion will be presented later in this report.

To gain information about the crystalline orientation, WAXD experiments were conducted with the X-rays passing along the ND. As expected, very strong crystalline orientation was observed for all the samples indicated by the

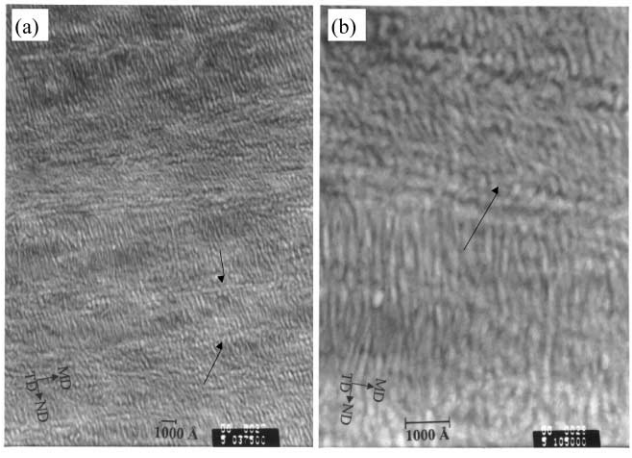

Fig. 7. The lower (a) and higher (b) resolution TEM of a typical MDO sheet showing the row-nucleated lamellar stacks. While the central shish-like structures remain well encapsulated by the stacks of lamellae, the arrows indicate the faint evidences of such structures.

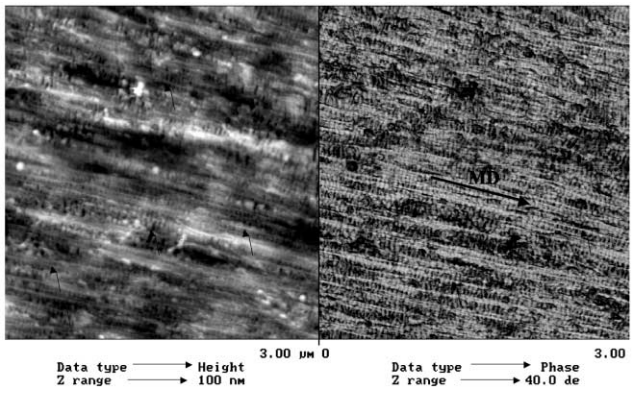

Fig. 8. AFM height and phase images of a typical MDO sheet. The size of the image is 3 μm × 3 μm. Notice the relatively smaller height profile for the MDO sheet compared to the spherulitic base sheet, indicating a much smoother surface morphology. In the phase image, the brighter regions represent the harder phase and usually correspond to the crystalline lamellae. The darker regions usually represent the softer amorphous phase. The arrows indicate the 'row-like' structures.

strongly defined and intense equatorial diffraction arcs of the (110) and (200) reflections. These results are in accordance with the DSC melting results and indicate more perfect crystals strongly oriented along the MD. However, no major differences were observed in the crystalline orientation among the various samples.

To better understand the nature of this crystalline orientation and the morphology of the MDO-sheet, TEM and AFM experiments were conducted and the results representative of all the MDO-sheet samples are reported in Figs. 7 and 8. The electron micrographs reveal highly developed stacks of lamellae that are oriented strongly along the MD. The AFM micrographs suggest that the majority of these lamellar stacks are nucleated from row crystals (akin to a shish–kebab morphology), while the TEM does not reveal the row structures to the same extent. The central row crystals, which are mostly well encapsulated by stacks of lamellae, are more easily detected by AFM than by TEM. The lateral width of most of these lamellae was observed to be in the range of 0.1–0.2 μm, though some regions revealed lamellae as long as 0.6 μm. The lateral widths attained by the lamellae depend upon the concentration of the rows from where these stacks of lamellae originate. The population of these rows is expected to relate to the amount of higher molecular weight chains present in the polymer as they are more likely to form the row-like crystals. It is useful to note that no significant twisting or curving of the lamellae was observed for the MDO-sheet samples as they were developed under high stress conditions. This is unlike the base sheet, which was developed under low stress isotropic conditions and demonstrated twisted lamellae. It is also seen that significant interlocking [27] of lamellae originating from different stacks take place. We did not observe any noticeable differences in the morphology across the thickness profile by TEM (microtoming was conducted closer to the two surfaces and also in the interior regions). It should

Table 1
Refractive indexes for the MDO sheets. For sample nomenclature, refer to Fig. 7

Sample	η_{MD}	η_{ND}	η_{TD}	η_{MDND}	η_{TDND}	η_{MDTD}
A	1.5704	1.5238	1.5268	0.0466	0.0030	0.0436
B	1.5700	1.5260	1.5281	0.0440	0.0021	0.0419
C	1.5704	1.5214	1.5254	0.0490	0.0040	0.0450
D	1.5704	1.5212	1.5250	0.0492	0.0038	0.0454
E	1.5707	1.5245	1.5270	0.0462	0.0025	0.0437

be noted that the TEMs presented here were obtained when the electron beam passed along the TD. The success of our TEM experiments depended largely on how closely we were able to microtome our samples perpendicular to the TD so that we could observe the morphology fully along the TD. Slight deviations from this orientation resulted in very poor contrast due to the nature of the morphology in the present case. Earlier attempts at looking along the MD direction resulted in failure as the contrast between the adjacent crystalline and amorphous regions developed by the staining technique was insufficient. This was because in this instance, the lamellar thickness direction is so well oriented along the MD that while looking along the MD, one looks at the lateral surfaces of the lamellae (flat on) and consequently a well-defined intervening amorphous phase boundary does not appear between the crystalline and the amorphous regions.

AFM confirms the observations from TEM and shows well-developed lamellar stacks along the MD on both surfaces of the MDO sheet. The fibril nuclei remain hidden under the lamellar stacks and are not distinctly revealed at the surfaces. The height images from the AFM reveal that the surface morphology of the MDO sheets is much smoother than the earlier base sheets. This is expected as stacked lamellae are expected to be much flatter than the spherulites of 3–5 μm size. However, it is interesting to consider why there were no substantial differences either in (a) the nature of stacking, (b) the thickness of the lamellae or (c) their orientation with respect to MD, even when the MDO temperature was varied from $T_{MDO} - 8°C$ to $T_{MDO} + 8°C$? Is the mechanical heat of drawing released when drawing 6*X* so high that the local temperature rises considerably above the melting point in all cases, or, is the transformation in fact a result of a continuous melting and recrystallization process? This issue will be examined in greater detail later in this paper when we halt the transformation process at several stages by systematically varying the MD draw ratios between 1.5*X* and 6*X*.

Table 2
Average density and crystallinity calculated from refractive indexes For sample nomenclature, refer to Fig. 7

Sample	Average η	Average density	X_c (%)	X_c (DSC) (%)
A	1.5403	0.961	69	64
B	1.5414	0.963	71	63
C	1.5391	0.959	67	72
D	1.5389	0.959	67	68
E	1.5407	0.962	70	67

Refractive index measurements along each of the three sample axes were conducted on MDO sheets for quantifying the overall average or system orientation. The results are presented in Table 1. The refractive index is dependent on the inherent polarizability characteristics of the repeat unit and is also sensitive to chain orientation of both the crystalline and the amorphous phase. For polyethylene, the highest refractive index is along the chain axis [36]. A very strong orientation along MD is indicated as the refractive index along that direction is significantly higher for all MDO-sheet samples. In resemblance to the earlier DSC, X-ray, TEM and AFM results, the birefringences were very similar for all MDO-sheet samples indicating the similarity in orientation among the MDO sheets that differed only in their cast roll and MDO draw temperatures. The average refractive index for the samples was computed ($(n_x + n_y + n_z)/3$) and used to calculate the average density using Schael's plot [36], which correlates closely with the well-known Lorentz–Lorentz relationship. The degree of crystallinity was calculated using the average density that extended from the average refractive index measurements. The DSC was run on exactly the same samples and the degree of crystallinity obtained by that technique is also shown in Table 2. The values of X_c derived from the refractive index measurements show a much narrower spread than what had been obtained from the DSC results. While refractive index measurement is a non-destructive method of evaluation, the DSC analysis results in reorganization during the heating scan and thus may not accurately represent the original sample. One may contest the values of X_c obtained from refractive index measurements as only representing the surface crystallinity. However, our morphological observations indicate that there seems not to be any significant differences across the thickness profile.

3.3. Biaxiality of the MDO process

For polyethylene, the refractive index along the chain direction is higher than the refractive index along its orthogonal directions. This is true for both the amorphous and orthorhombic crystalline phase in polyethylene. Thus, considerably higher refractive index along the MD can be related to increase in overall chain orientation along that direction. In this regard, it is noticed that for the MDO sheets, the refractive index along the TD direction is always noticeably more than that along the ND. For purely uniaxial orientation along MD, the refractive index along the TD and ND are expected to be equal. However, the definite difference in these values as given by $\Delta_{TD,ND}$ indicates the slight biaxiality of this orientation process. This indicates that the drawing of the MDO sheets is not purely uniaxial, but has a small biaxial component to it. This result cannot be readily

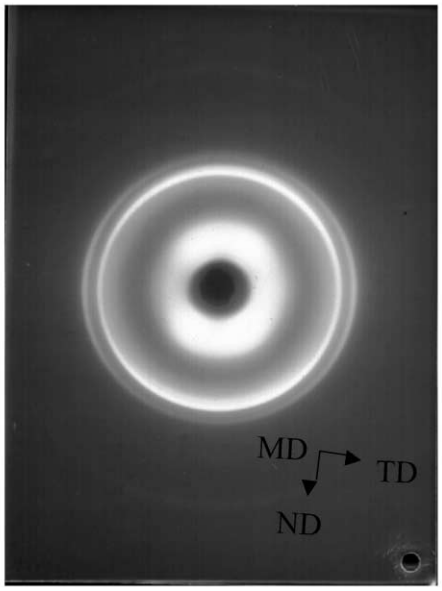

Fig. 9. WAXD image of a MDO sheet drawn 6*X* when the X-ray passes through the MD. Orientation along the TD indicates the biaxiality of the MDO process.

gauged from our earlier results or from the morphological observations by AFM or TEM. To test the validity of this interpretation, we conducted X-ray experiments on the MDO sheets in which the X-ray was passed parallel to the MD (Fig. 9). The azimuthal dependence of the reflections reveals a noticeable preferential orientation of the crystal '*a*-axis' along the ND, while the '*b*-axis' is preferentially oriented along the TD. These results directly support the conclusion derived from the refractometry experiments.

The reason for this TD orientation is related to the manufacturing process where the draw in the MD takes place using a set of three heated rolls placed very close to each other. During the drawing process, the sheet is in tight contact with the rolls due to the tension in the manufacturing line. This tight contact between the rolls and the sheet is a necessary requirement for carrying out the drawing effectively and also to prevent any sagging or droop in the manufacturing line.

We know, however, that the density of the polymer does not change appreciably as indicated by the crystallinity measurements. The volume thus remains nearly the same (volume = mass/density) during the drawing process. Thus, as the sheet is stretched 6*X* along the MD, contraction in the TD and ND will normally take place. For a freely standing film, the amount of this contraction would be equal along the TD and ND. However, the tight contact between the rolls and the sheet in the present case principally only allows planar extension and prevents the sheet from contracting along the TD. The contraction only takes place along ND thereby resulting in an MDO sheet that is one-sixth as thick as the precursor base sheet. A TD stress is therefore developed that leads to the biaxiality in the orientation process. As a tight contact of the sheet is usually necessary, we suspect that the feature of biaxiality will thus be present in other similar commercial tenter-frame MDO processes.

3.4. Transformation to the stacked lamellar structure

As discussed earlier, the overall goal of this work had been to enable a better control of the manufacturing process in terms of identifying the key variables that influence the morphology and orientation behavior. In this regard, we notice that the cast-roll temperatures did not produce any major differences in the morphology of the various base sheets. We also note that the morphology and orientation of the MDO sheets remained largely unaffected when the MDO draw temperature is varied over the temperature range of 18°C (T_{MDO} − 8°C to T_{MDO} + 8°C)). While the morphological and orientation behavior of the base sheets and MDO sheets were distinct, the question of how this transformation took place remained unanswered. It was nonetheless noticed that MDO-sheet morphology gave no evidence of any remnants of the previous spherulitic superstructure. It is impossible to visualize that the spherulitic lamellae will deform and rearrange, without melting, into such a neatly stacked lamellar structure! It is therefore clear that the spherulitic superstructure is completely destroyed during the drawing process. During the different stages of this spherulitic deformation, various deformation modes such as lamellar shear, lamellar separation and lamellar rotation are expected to be operable before the lamellae are broken/destroyed. While these deformation stages have been extensively discussed by others [37–47], our interest presently concerns the stages subsequent to these, namely, (a) how does the stacked lamellar structure result, post-destruction of the spherulitic lamellae, and (b) what is the size scale of this destruction and melting process, i.e. is it localized melting or bulk melting? In this regard, it is important to look at this transformation as potentially arising from three distinct routes:

(1) The drawing temperatures utilized are well above the general range of temperatures associated with the α_c relaxation whose origin is associated with mobility within the crystal. In fact, the drawing temperatures, it is recalled, are located at the beginning and well into the primary melting endotherm of the HDPE base sheet. It has been demonstrated by other workers [48] that the polyethylene lamellae show enhanced crystal perfection and thickening at temperatures close to the melting point due to the ability of the crystal phase to reorganize. At these temperatures then, the high-speed deformation of HDPE to a high draw ratio (6*X* in this case) can be expected to result in large-scale spherulitic disruption and breakup of chain folded lamellae. On a microscopically localized scale, the spherulitic lamellae that are partially destroyed/melted, continuously convert to a microfibril. This is followed by the subsequent melting and recrystallization of the nearby polymer in the form of lamellar stacks oriented along the MD and connected by the

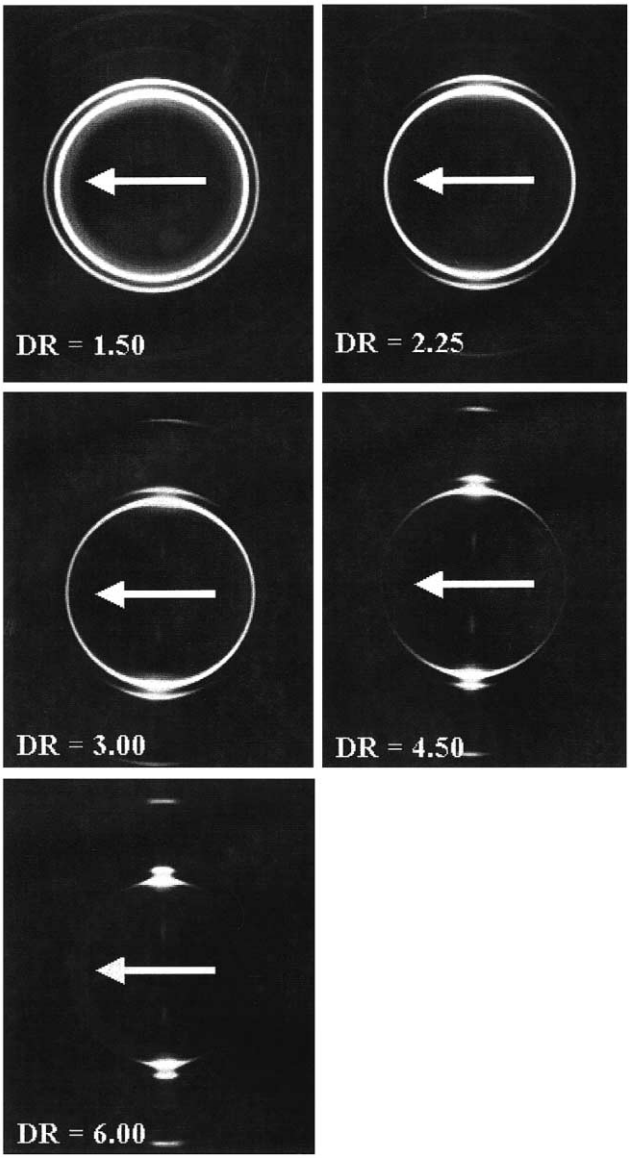

Fig. 10. WAXD images for MDO sheets drawn to various ratios. The arrows indicate the MD.

microfibril. It may thus be visualized that this continuous breakup of spherulites accompanied by the partial melting and recrystallization processes leads to the final neatly microfibrillar stacked lamellar morphology. The essential features of this model are the continuity of the transformation during the drawing process and the coexistence of the previous spherulitic lamellae, the deformed/melted lamellae and microfibrillar lamellar stacks during the transformation process.

(2) When the drawing is carried out at very high draw rates and to a high draw ratio, such as in this study, significant energy of elastic and plastic deformation is released. If good heat transfer conditions exist, then this energy of drawing can be quickly dissipated. However, in the present case, when the polymer sheet is so thick and when the draw is carried out at such high draw rates, the energy of drawing is not expected to quickly dissipate. This can then lead to significant temperature rise and thus large-scale bulk melting of spherulites can occur. This second viewpoint is plausible in lieu of the position of the drawing temperatures vis-à-vis the primary melting endotherm of HDPE. As all the drawing temperatures are located in the region of bulk melting of polyethylene, the additional temperature rise resulting from the energy of drawing may take the polymer into a completely melted state. A row-nucleated stacked lamellar structure can then develop from this oriented liquid-like state. We here draw a distinction between a row-nucleated structure (envisioned to occur from the melt) and microfibrillation (for which complete melting is not necessary).

(3) A final scenario which is a combination of the above two models can exist. While some regions of the sample may experience bulk melting and subsequent row-induced crystallization (model 2), other regions may continuously transform by the localized partial melting and microfibrillar recrystallization (model 1). The likelihood of bulk melting would be higher in the central regions of the sheet from where the heat of melting may not dissipate quickly.

It was therefore realized that some key-processing variable needed to be systematically varied to gain a better understanding of the dramatic change in morphology that occurs during the drawing process. In this regard, the 'draw ratio' was selected as a variable and was systematically changed from 1.5*X*, 2.25*X*, 3*X*, 4.5*X* to 6*X*. It was thought that by altering the draw ratio in this systematic manner, the drawing process could be halted at various stages of deformation and thus the transformation process could be better understood. We first report on the results from various techniques on the samples that differed in the amount of uniaxial draw.

3.5. Effect of MD draw ratio on crystalline orientation

Wide-angle X-ray diffraction experiments were performed on the samples drawn to different ratios at room temperature with the X-ray beam parallel to the thickness direction (perpendicular to the MD). The successive WAXD patterns (Fig. 10) reveal a very clear and systematic increase in the degree of crystalline orientation as the draw ratio was increased from 1.5*X* to 6.0*X*. The (110) and (200) diffraction rings observed in the WAXD of a 'base sheet' progressively sharpen and convert to very defined and intense equatorial arcs as the draw ratio is increased. In fact, the weaker (020) reflection is also visible on the X-ray patterns and it also progressively sharpens along the equatorial direction as the draw ratio is increased to 6*X*. Based on the earlier microscopy experiments and these X-ray results, some deductions about the orientation of the three orthogonal axes *a*, *b* and *c* can be made. We know from previous morphological results using AFM and TEM that a row-induced and very well-stacked lamellar structure develops in the films drawn 6*X* so that a strong

c-axis orientation along the MD direction is expected. The X-ray experiments reveal the nature of the (200) and (020) planes and suggest that both the *a*-axis and *b*-axis are preferentially oriented perpendicular to the MD. However, the *a*-axis seems to be more prominently oriented perpendicular to the MD than the *b*-axis as indicated by the sharper azimuthal dependence of the (200) planes compared to (020) planes. The near perpendicular orientation of the (110) planes also supports this conclusion about the orientation of the *a*- and *b*-axes. It was also shown earlier in Fig. 9 (which revealed the biaxiality of the MDO process) that the *a*-axis has a preferential orientation along the ND.

For oriented HDPE films, a stress-induced martensitic transformation, in which the orthorhombic structure of the unoriented PE is converted to a monoclinic structure, has been reported in the literature [49,50]. It has been argued that this monoclinic phase may be an intermediate step in the crystal deformation and could occur due to fold-plane transitions above a critical shear stress. This transformation, however, should be accompanied by the appearance of additional reflections in the WAXD pattern, which are not observed in data. This could very well be due to high temperature of drawing for the present samples, where the monoclinic phase is expected to be unstable and convert to the orthorhombic phase. It is also possible that the monoclinic structure may not have formed in the present case.

3.6. Morphological results from the AFM

Selected AFM results are reported for various MDO sheets drawn to different ratios (Fig. 11a–e). As stated earlier, a coarsely developed spherulitic morphology was observed for the base sheet. For the MDO-sheet sample drawn 1.5*X*, the spherulitic structure, which was of the order of 3 μm, seems to be very disrupted as there is no evidence of it in both the lower resolution (10 μm, not shown here) and higher resolution (3 μm, Fig. 11a) scans. Furthermore, the original lamellar stacks in the spherulites seem to be largely broken/deformed. No well-stacked row-nucleated lamellae structures (that are found in the MDO sheets drawn 6*X*) are observed. In fact, in some regions, the lamellae are oriented along the MD so that the chain direction is almost perpendicular to the MD! Finally, the lamellae do not lie preferentially 'edge on' (as was the case in the MDO sheet drawn 6*X*) but may also be 'flat on' in many regions.

For the MDO sheet drawn 2.25*X*, the morphology shows a change in that the stacked lamellar structures begin to appear. The overall morphology is very complex and is akin to a collage of largely deformed lamellae dispersed with some stacked lamellar structures. No large-scale morphological superstructures are present. We believe that this morphology is partially microfibrillar. It is also noticed that the 'fibrils', associated with the stacked lamellae, are comparable in thickness to the lamellae that are present elsewhere. While the deformed spherulitic lamellae are dispersed in several directions, the stacked lamellae are always very well aligned along the MD. A similar trend continues when we examine the morphology for the MDO samples drawn 3*X*. The population of stacked lamellar structures shows an appreciable increase. The population of deformed lamellae, which are remnants of the spherulitic morphology of the base sheet, is largely decreased. It is, however, very clear that at least for samples deformed 2.25*X* or 3*X*, no large-scale bulk melting has taken place during the deformation process. Such bulk melting, if it had occurred, would have destroyed the lamellar structures reminiscent of the spherulitic morphology to a large extent. For both these samples, the lateral width of the lamellae seems to be limited to less than '0.1 μm' due to the existence of other deformed lamellae or the high packing density of the extended chain fibrils.

For the MDO-sheet samples drawn 4.5*X*, the morphology is better defined as it is now distinctly dominated by the population of stacked lamellar structures and contains a lesser number of deformed/broken lamellar structures. The stacked lamellar structures are even better defined for samples drawn 6*X*, with very little or no reminiscence of previous spherulitic morphology present. For both these samples, the lateral width of the lamellae is less than 0.1 μm. Also, the fibrils in the center of the stacked lamellar structures are much finer than for the samples drawn 2.25*X* or 3*X*.

3.7. Morphological results from the TEM

We next examine the TEMs for samples drawn to various ratios (Fig. 12 a–f). The samples that were drawn 1.5*X* (Fig. 12a) show high deformation of the original spherulitic structure. Spherulitic boundaries that were well defined in the base sheet are more diffuse in the samples drawn 1.5*X*. In agreement with AFM results, no evidence of any microfibrillation is found. It is also observed that deformation is most prevalent in the equatorial and polar region of the spherulites (where the lamellae are perpendicular and parallel respectively to the MD), whereas the central and regions at 45° are still intact to a large extent. For samples drawn 2.25*X* (Fig. 12b), the results remain in agreement with the AFM results in that much of the previous spherulitic structure is destroyed and stacked lamellae structures begin to appear. Only the center of the spherulites and few of the lamellae at 45° remain as indicated by the 'X' shaped structures (Fig. 12b). The trend towards increasing stacked lamellar population continues for the samples drawn 3*X* (Fig. 12c) and 4.5*X* (Fig. 12d). The observations indicate the increase in either microfibrillation or row nucleation and only faint reminiscences of the previous spherulitic structure. The samples drawn 6*X* (Fig. 12e) provide the best-defined morphology in terms of a well-developed stacked lamellae structure and almost complete destruction of the previous lamellae. Between the various samples, no noticeable differences could be observed

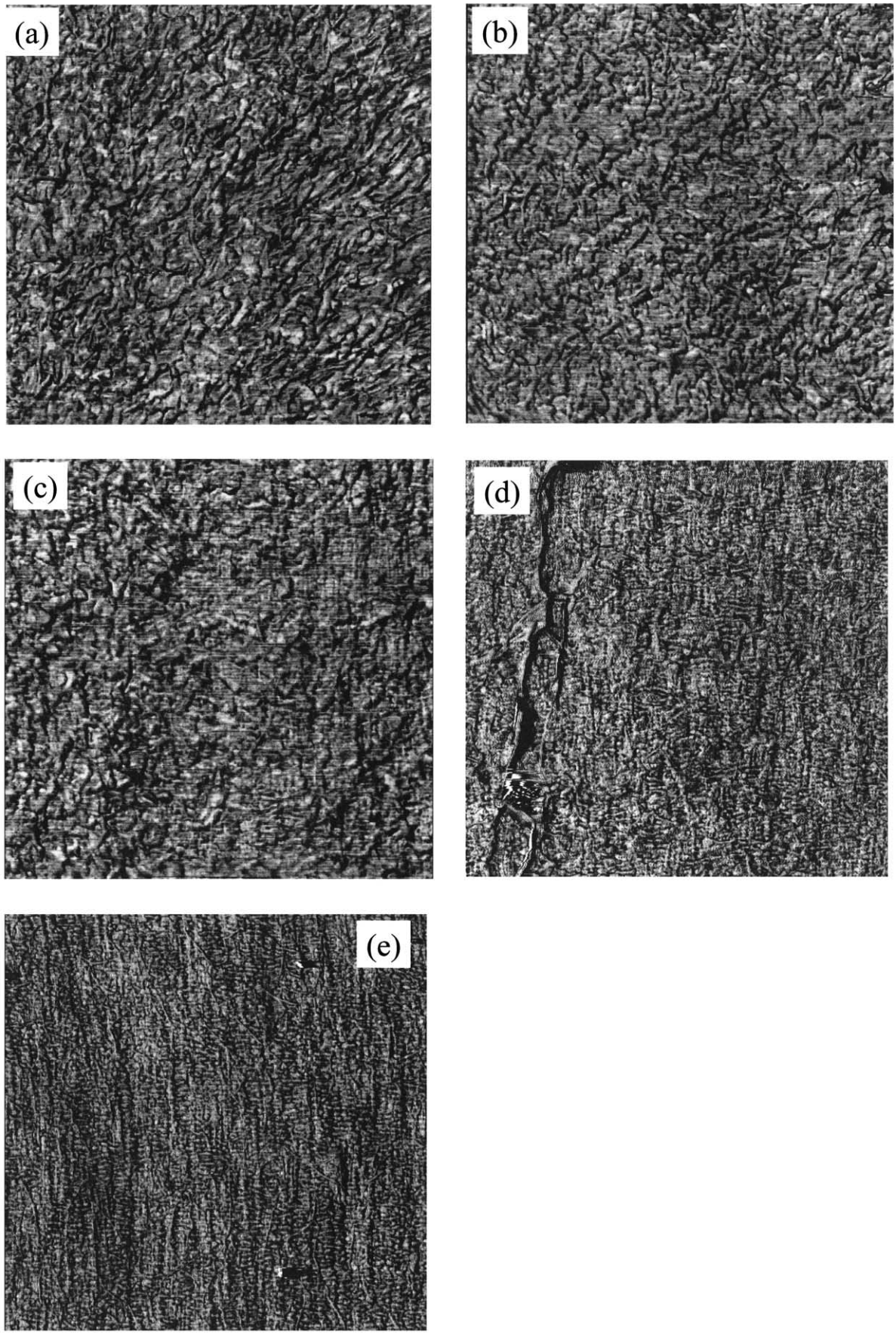

Fig. 11. AFM images for MDO sheets drawn to various ratios. The MD direction is along the vertical. The draw ratios are (a) 1.5*X*, (b) 2.25*X*, (c) 3*X*, (d) 4.5*X* and (e) 6*X*.

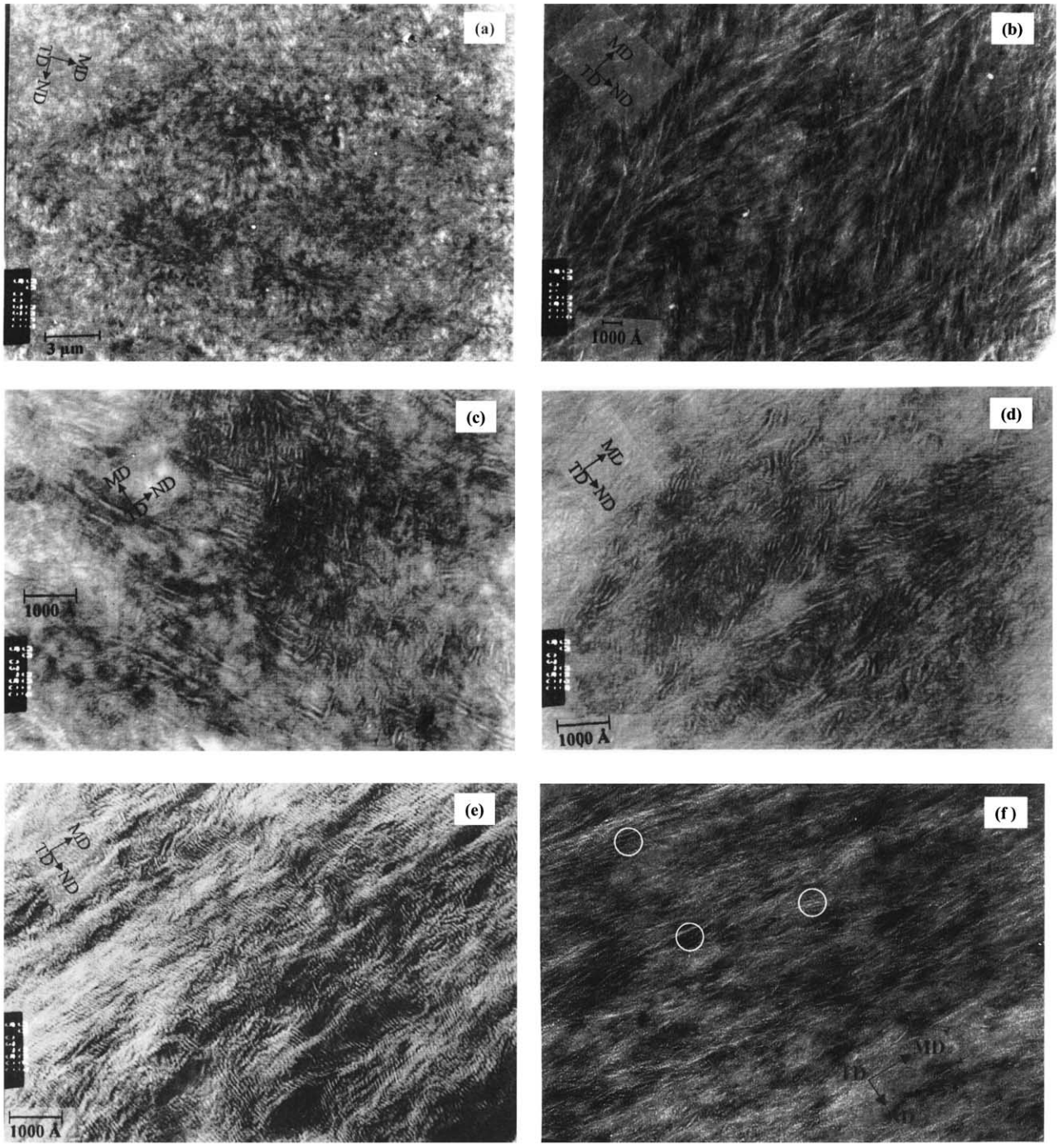

Fig. 12. TEM images for MDO sheets drawn to various ratios. The draw ratios are (a) 1.5*X*, (b) 2.25*X*, (c) 3*X*, (d) 4.5*X*, (e) 6*X* and (f) magnified 6*X* highlighting the visible 'row' structures.

in the lamellar thickness or the lateral width of the stacked lamellar structures. It may be interesting to explore in the future how draw ratios greater than '6*X*' may affect the morphology in terms of the thickness of the lamellae and their lateral width.

On the basis of both AFM and TEM results, we feel confident in stating that large-scale bulk melting, although possibly occurring to some extent for higher draw ratios, is not necessary for developing the stacked lamellar structures. The stacked lamellar structures begin to appear due to localized melting and recrystallization (microfibrillation) even at draw ratios of 2.25*X*. The amount of microfibrillation continues to increase for higher draw ratios, at which stage we believe some degree of bulk melting occurs leading to row-nucleated stacked lamellar structures.

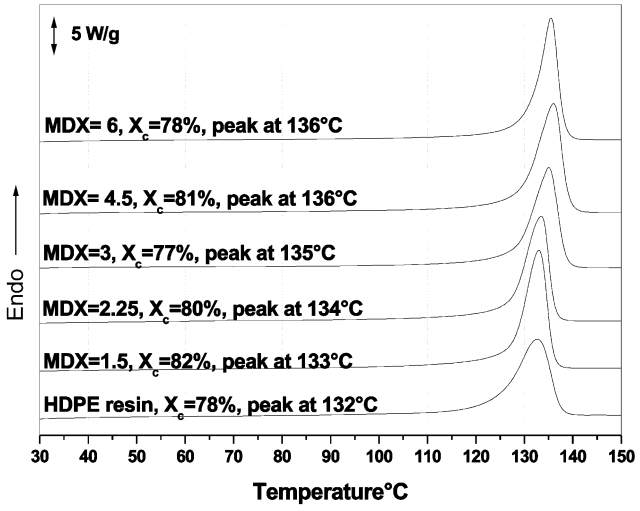

Fig. 13. DSC heating scans for the HDPE resin and the MDO samples drawn to various draw ratios. The draw ratio, the calculated degree of crystallinity and the peak melting temperatures are indicated in the figure.

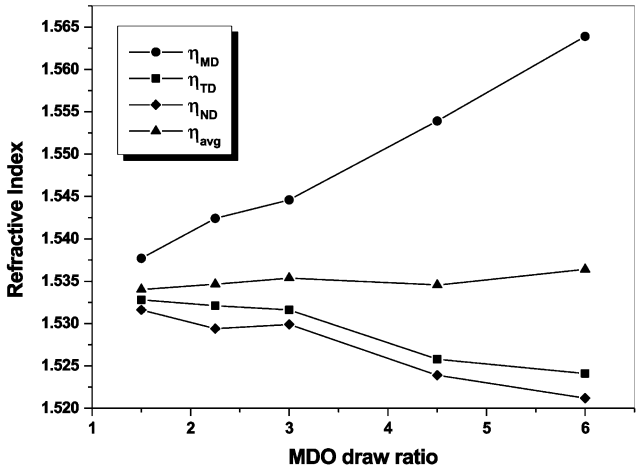

Fig. 14. The refractive index of the MDO sheets versus the draw ratio. Both the average and the directional refractive indexes are illustrated.

3.8. Effect of draw ratio on overall orientation

DSC heating scans conducted for the samples drawn to different ratios at 30°C/min are shown in Fig. 13 that also illustrates the position of the draw temperature relative to the melting profile. It is clear that higher draw ratios systematically result in more perfect crystals with narrower melting distribution as indicated by the breadth of melting. This difference in breadth of melting is clearly realized for the unoriented HDPE resin and the sample drawn 1.5*X*. The DSC experiments in this case relate the narrowing of melting distribution to the more uniform lamellar thickness observed by microscopy results. The faster heating rate was thus used to minimize the reorganization effect in these oriented samples. This may, however, lead to slightly higher thermal lag, and thus, the values of peak melting point should be considered approximate. The values of X_c obtained were ca. 77–82% for all the drawn samples, this variation being within the range of error associated with our experiment.

Refractive index measurements were performed on the drawn HDPE sheets (Fig. 14). It is observed that the average refractive index does not change noticeably with increasing draw rates, thereby indicating that the degree of crystallinity is not affected by drawing. While a substantial transformation of the morphology occurs by localized deformation, melting and recrystallization processes, the amount of crystallinity remains relatively unchanged. A similar conclusion is reached on the basis of DSC results (not reported here). It is, however, clear that the refractive index in the MD increases significantly with increasing draw ratios. While there will be a small contribution due to the amorphous orientation, the bulk of this increase is due to the increasing crystal orientation along the MD. It is also noticed that, in general, the three refractive indices are most affected when the draw ratio is 4.5*X* and 6*X*. In conjunction with the morphological results, this large increase in refractive index corresponds with complete destruction of the spherulitic morphology and occurrence of well-developed stacked lamellar morphology. On drawing most chains begin to orient towards the MD, and thus, there is a corresponding decrease in the refractive indexes along the TD and ND directions. It is also interesting to observe that there is always a higher refractive index for the TD than for ND direction (i.e. $\Delta_{TD,ND} \neq 0$), indicating that overall, there is slight biaxiality for all draw ratios. This result is accordance with the X-ray results that had revealed the biaxial nature of this MDO drawing process. Higher draw ratios lead to higher stress along the TD resulting in higher $\Delta_{TD,ND}$

4. Conclusions

Morphology of HDPE base sheets is unoriented and spherulitic with no differences in spherulite size (3–5 μm) across the thickness of the base sheet. However, a distinct change to a stacked lamellar morphology takes place when this base sheet is drawn 6*X* using a set of rolls. Draw temperatures, which lie in the vicinity of bulk melting of polyethylene, are very important in facilitating this change by enabling localized melting and recrystallization (microfibrillation) of the spherulitic lamellae into lamellar stacks oriented perpendicular to MD. However, in the range of base sheet and MDO draw temperatures studied, no appreciable differences could be observed in the overall orientation or morphology of the MDO sheets. This is an important observation from manufacturing standpoint as it enables a

bigger processing window for drawing operations. Another noteworthy feature of the drawing process is the slight biaxiality introduced along the TD. This occurs due to a slight TD stress that develops when the transverse movement of the film is prevented due to it being pinned down against the rolls. The very detailed morphological observations fail to provide any evidence of this biaxiality that, however, is clearly revealed by WAXD and refractive index measurements.

The systematic variation of the draw ratio to 1.5*X*, 2.25*X*, 3*X*, 4.5*X* and 6*X* at a temperature in the region of the lower portion of the melting endotherm leads to the stepwise deformation and distribution of the original spherulitic superstructure. At low draw ratios, the destruction of the bulk spherulites took place resulting in broken and deformed lamellar remnants, most of which were oriented roughly at 45° to the draw direction. With higher draw ratios, the stacked lamellar structures begun to sporadically appear due to localized melting of the weaker and thinner crystals and the subsequent microfibrillation. The population of these lamellar stacks that were oriented perpendicular to the draw direction increased for higher draw ratios until the morphology was dominated by such structures for samples drawn 6*X*. As this change in morphology took place, the increase in overall and crystalline orientation was indicated by refractive index and X-ray experiments, respectively. It is clear that MD draw ratio serves as a key variable in enabling the stacked lamellar morphology to develop while varying the MDO draw temperature makes little difference in orientation and morphology in the range of draw temperatures studied.

Acknowledgements

The authors wish to thank the Exxon Mobil Chemical Company for complete financial support of this work and also for manufacturing the sample at their film division in Macedon, NY.

References

[1] Osborn KR, Jenkins WA. Plastic films — technology and packaging applications. Lancaster: Technomic, 1992.
[2] Mount III EM. Polyolefins RETEC, February 1999.
[3] Kanai T, Campbell A, editors. Film processing Munich: Hanser, 1999.
[4] Yu TH, Wilkes GL. Polymer 1996;37:4675 [Erratum 1997;38(6): 1503].
[5] Yu TH, Wilkes GH. J Rheol 1996;40:1079.
[6] Yu TH, Wilkes GL. J Plast Film Sheet 1997;13:299.
[7] Zhou H, Wilkes GL. J Mater Sci 1998;33:287.
[8] Butler MF, Donald AM. J Appl Polym Sci 1998;67:321.
[9] Pazur RJ, Prud'homme RE. Macromolecules 1996;29:119.
[10] Pazur RJ, Prud'homme RE. J Polym Sci, Part B 1994;32:1475.
[11] Hofmann D, Geiss D, Janke A. J Appl Polym Sci 1990;39:1595.
[12] Kurtz SJ. Int Polym Process 1995;2:148.
[13] Ma TC, Han CD. J Appl Polym Sci 1988;35:1725.
[14] Feijoo JL, Sanchez JJ, Muller AJ. Polym Bull 1997;39:125.
[15] Kim YM, Kim CH, Park JK, Lee CW, Min TI. J Appl Polym Sci 1997;63:289.
[16] Heffelfinger CJ, Burton RL. J Polym Sci 1960;47:289.
[17] Nie HY, Walzak MJ, McIntyre NS. Polymer 2000;41:2213.
[18] Benning CJ. Plastic films for packaging. Technomic, 1983.
[19] Peterlin A. Colloid Polym Sci 1975;253:809.
[20] Peterlin A. J Mater Sci 1971;6:490.
[21] Hay IL, Keller A. J Mater Sci 1966;1:41.
[22] Hay IL, Keller A. J Mater Sci 1967;2:538.
[23] Hay IL, Keller A. J Mater Sci 1968;3:646.
[24] Hay IL, Keller A. J Mater Sci 1969;4:908.
[25] Stein RS, Norris FH. J Polym Sci 1956;21:381.
[26] Ward IM, editor. Structure and properties of oriented polymers. New York: Chapman & Hall, 1997.
[27] Keller A, Kolnaar JWH. Prog Coll Polym Sci 1993;992:81.
[28] Samuels RJ. Structured polymer properties. New York: Wiley, 1974.
[29] Lin L, Argon AS. J Mater Sci 1994;29:294.
[30] Bowden PB, Young RJ. J Mater Sci 1974;9:2034.
[31] White JL, Cakmak M. Orientation processes. In: Mark HF, Bikales NM, Overberger CG, Menges G, Kroschwitz JI, editors. Encyclopedia of polymer science and engineering, vol. 10. John Wiley and Sons, 1987. p. 619.
[32] Sawyer LC, Grubb DT. Polymer microscopy. London: Chapman & Hall, 1987.
[33] Kanig G. Prog Coll Polym Sci 1975;57:176.
[34] Hodge AM, Bassett DC. J Mater Sci 1977;12:2065.
[35] Grubb DT, Keller A. J Polym Sci, Part B 1980;18:207.
[36] Pepper RE, Samuels RJ. In: Mark HF, Bikales NM, Overberger CG, Menges G, Kroschwitz JI, editors. Refractometry. Encyclopedia of polymer science, vol. 14. John Wiley and Sons, 1988. p. 289.
[37] Pope DP, Keller AJ. J Polym Sci 1975;13:533.
[38] Keller A, Pope DP. J Mater Sci 1971;6:453.
[39] Cayrol B, Petermann J. J Polym Sci, Part B 1974;12:2169.
[40] Cowking A, Rider JG, Hay IL, Keller A. J Mater Sci 1968;3:646.
[41] Tagawa T, Ognra K. J Polym Sci, Part B 1980;18:971.
[42] Peterlin A. Polym Engng Sci 1978;18:488.
[43] Prevorsek DC, Chin HB, Murthy S. ACS Prepr PMSE 1993;70:43.
[44] Fischer EW, Goddar HJ. J Polym Sci, Part C 1969;16:4405.
[45] Porter RS. ACS Polym Prepr 1971;12(2):39.
[46] Clark ES, Scott LS. Polym Engng Sci 1974;14:682.
[47] Clements J, Jakeways R, Ward IM. Polymer 1978;19:639.
[48] McCrum NG, Read BE, Williams G. Anelastic and deilectirc effects in polymeric solids. New York: Wiley, 1967.
[49] Cowking A, Rider JA. J Mater Sci 1969;4:1051.
[50] Hay IL, Keller A. J Polym Sci, Part C 1970;30:289.